Characterization by ^{27}Al NMR, X-ray Absorption Spectroscopy, and Density Functional Theory Techniques of the Species Responsible for Benzene Hydrogenation in Y Zeolite-Supported Carburized Molybdenum Catalysts

Angela S. Rocha,[†] Victor Teixeira da Silva,[‡] Jean G. Eon,[§] Sônia M. C. de Menezes,[||] Arnaldo C. Faro, Jr.,*[,†] and Alexandre B. Rocha[†]

Departamento de Físico-Química and Departamento de Química Inorgânica, Instituto de Química, UFRJ, Ilha do Fundão, CT, Bloco A, Rio de Janeiro, RJ, CEP 21949-900, Departamento de Engenharia Química, IME, Praça General Tibúrcio, 80 Praia Vermelha, Rio de Janeiro, RJ, CEP 22290-270, and PETROBRAS, CENPES, Ilha do Fundão, Quadra 7, Rio de Janeiro, RJ, CEP 21949-900, Brazil

Received: February 23, 2006; In Final Form: June 2, 2006

Carburized molybdenum catalysts supported on a dealuminated NaH−Y zeolite were prepared by carburization under a 20% methane in hydrogen flow of two precursors obtained by adsorption of molybdenum hexacarbonyl, one containing 5 wt % and the other 10 wt % Mo, and a third one was prepared by impregnation with aqueous ammonium heptamolybdate, containing 5 wt % Mo. The three catalysts displayed very distinct behaviors in the benzene hydrogenation reaction at atmospheric pressure and 363 K. By using XANES spectroscopy at the molybdenum L edge, EXAFS and XANES spectroscopy at the molybdenum K edge, and ^{27}Al solid-state NMR spectroscopy, it was shown that different carburized molybdenum species exist in each sample. In the catalyst containing 10 wt % Mo, formation of molybdenum carbide nanoparticles was observed, with an estimated diameter of 1.8 nm. In the catalyst containing 5 wt % Mo and prepared by carburization of adsorbed molybdenum hexacarbonyl, formation of molybdenum oxycarbide dimers is proposed. In the latter case, density functional theory calculations have led to a dimer structure which is compatible with EXAFS results. In the catalyst prepared by impregnation with ammonium heptamolybdate solution followed by carburization, the molybdenum seems to interact with extraframework alumina to produce highly disordered mixed molybdenum−aluminum oxycarbides.

1. Introduction

Transition-metal carbides, especially those of molybdenum and tungsten, have been frequently investigated as alternatives to platinum-group metal catalysts in industrially important reactions, such as hydrogenation, isomerization, and hydrogenolysis of hydrocarbons.[1−4]

Difficulty to control the textural properties of bulk carbides is one of the major problems concerning the use of these materials as catalysts. This can be circumvented by depositing the active phase on an adequate support. Zeolites are exceedingly important support materials, due to their high surface area and regular pore structure with molecular dimensions. This allows the preparation of highly dispersed supported phases and the molecular sieve action of zeolites to be taken advantage of to control catalyst selectivity and stability. Furthermore, the acidity of zeolites can be easily controlled by varying the Si/Al ratio and the amount of appropriate charge-compensating cations. Nevertheless, there are few studies on the preparation and properties of zeolite-supported carbides, most of them concerned with the use of molybdenum carbide supported on ZSM-5 for methane dehydroaromatization.[5−9]

In the petroleum-refining industry, Y zeolite is widely used as a support for platinum-group metals in hydrocracking and hydrodearomatization processes.[10,11] In the former case, use is made of the bifunctional character of zeolite-supported metal catalysts. In the latter, it is known that the sulfur tolerance of metals is improved when deposited in a highly dispersed form on acidic supports.[10−12] The work reported in the present paper is part of a project which aims to investigate carburized molybdenum as a possible alternative to platinum-group metals as the hydrogenating component in Y zeolite-supported catalysts.

We have recently shown[13] that Y zeolite-supported carburized molybdenum is active in benzene hydrogenation at low temperature (363 K) and atmospheric pressure. The catalysts were prepared by adsorption of molybdenum hexacarbonyl vapors at 343 K, followed by temperature-programmed carburization under a 20% methane in hydrogen mixture up to 923 K. For the same silica/alumina ratio (SAR), activity increased with increasing sodium content and, for low sodium contents, with increasing SAR. Controlled reoxidation of the catalysts clearly established that initial catalytic activity was strongly favored by concurrent low average molybdenum oxidation state (<4) and carbon incorporation (Mo/C ratio < 4). Besides, low average molybdenum oxidation states were favored by higher SAR and higher sodium content of the zeolite supports, suggesting that protonic acidity of the zeolite is detrimental to the formation of reduced molybdenum species during carburization. Additionally, a catalyst prepared by carburization of a precursor obtained by impregnation with ammonium heptamolybdate (AHM) solution presented a higher activity as compared to the other catalysts. However, the nature of the species responsible for

* To whom correspondence should be addressed. E-mail: farojr@iq.ufrj.br.
[†] Departamento de Físico-Química, Instituto de Química, UFRJ.
[‡] IME.
[§] Departamento de Química Inorgânica, Instituto de Química, UFRJ.
[||] CENPES.

10.1021/jp061153x CCC: $33.50
Published on Web 07/25/2006

benzene hydrogenation and the reasons for the observed differences in catalytic activity were not clarified.

In the present work, the effects of molybdenum loading (5 or 10 wt %) and the method of molybdenum incorporation (adsorption of molybdenum hexacarbonyl or impregnation with AHM solution) on benzene hydrogenation activity and stability are investigated for catalysts supported on a dealuminated Y zeolite. The catalysts were characterized by EXAFS at the molybdenum K edge and XANES at the molybdenum K and L edges, as well as by ^{27}Al solid-state NMR, to elucidate the nature of the molybdenum species formed by carburization. Density functional theory (DFT) was used to check the viability of some proposed species.

2. Experimental Section

2.1. Preparation of the Catalysts. A dealuminated and partly protonic Y zeolite, NaHY-9, used as the support was provided by the PETROBRAS R&D Centre, CENPES. It has the following properties: 2.13 wt % Na, 615 $m^2\ g^{-1}$ BET surface area, framework silica/alumina ratio 9.2 (from FTIR), and 33% of the aluminum as extraframework alumina (EFAL).

Two precursors were obtained by adsorption of molybdenum hexacarbonyl, following the method described by Zotin.[14] The zeolite was first dried under vacuum at 673 K for 4 h. Without further exposure to air, it was mixed under argon with a sufficient amount of molybdenum hexacarbonyl to produce catalysts containing 5 or 10 wt % Mo. The mixture was heated under vacuum at 343 K for 16 h in a closed reactor. Under this condition, the sublimation of $Mo(CO)_6$ followed by the adsorption on the zeolite takes place. Any nonadsorbed carbonyl was removed by evacuation at room temperature. A third precursor was prepared by multiple wet point impregnations of the zeolite with an aqueous solution of AHM, followed by drying at 393 K for 2 h and calcination at 673 K for 4 h, to obtain a catalyst with 5 wt % Mo.

The carburization procedure for these precursors was described in a previous paper.[13] Briefly, the precursors were carburized under a 150 $cm^3\ min^{-1}$ flow of a mixture containing 20% methane in hydrogen up to a temperature of 923 K at a 10 K min^{-1} heating rate. The final temperature was kept for 1.5 h. The carburized catalysts prepared by adsorption were named 5MoC/NaHY-9 and 10MoC/NaHY-9, and the one prepared by impregnation was named 5MoCI/NaHY-9.

2.2. Catalytic Test: Benzene Hydrogenation. The catalytic test was performed at atmospheric pressure, under a 30 cm^3 min^{-1} flow of hydrogen saturated with benzene vapor at 296 K ($p_V = 11.3$ Pa), at a 363 K reaction temperature, and with 0.25 g of catalyst. The composition of the reactor effluent was followed on line, by means of a Finnigan 9001 gas chromatograph. Cyclohexane was the only product observed under these conditions.

2.3. Characterization. Surface areas were determined from nitrogen adsorption isotherms at 77 K using the BET method, in an ASAP 2010 volumetric apparatus. Before the analyses, the materials were pretreated under vacuum at 673 K.

The carbon content of the catalysts was determined via the amount of carbon dioxide produced during the reoxidation of the carburized material at 873 K under a mixture of oxygen and helium in a glass system with recirculation of the gas phase, as described previously.[13]

The carbon monoxide chemisorption measurements were carried out in a Micrometrics ASAP 2010 volumetric apparatus, with in situ carburization. Two isotherms were acquired for each catalyst at 308 K with intermediate evacuation for 0.5 h, and the amount of chemisorbed CO was obtained by the method of isotherm subtraction.

The ^{27}Al NMR MAS (magic angle spinning) spectra for the materials were recorded with a Varian INOVA-300 (7.05 T magnetic field) instrument, equipped with a solid sample probe, in zirconia 7 mm rotors, with an MAS spinning rate of 6 Hz. The measurements were performed by using radio frequency pulses of 0.7 μs ($\sim\pi/20$), separated by 0.3 s, and 6000 transients were collected. All spectra took $AlCl_3 \cdot 6H_2O$ (0 ppm) as the reference.

The X-ray absorption (XAS) measurements were performed at the molybdenum K edge, at the Laboratório Nacional de Luz Síncronton, LNLS, Campinas, Brazil. The spectra were recorded at room temperature in transmission mode, using a 0.5 mm slit opening and a Si(220) monochromator, without exposure to air after carburization, making use of acrylic cells sealed with Kapton tape. All sample manipulation was made under an argon atmosphere in a drybox. The intensities of the incident and transmitted beams were monitored by ionization chambers filled with argon.

In the XANES measurements at the molybdenum K edge, three scans were taken in the range 19930−20200 eV. From 19930 to 19988 eV, 2 s and 2.0 eV steps were used, from 19990 to 20049 eV, 2 s and 1.0 eV were used, and from 20050 to 20200 eV, 3 s and 2.0 eV were used. The EXAFS scans were performed in the range 19900−21200 eV. From 19900 to 20148 eV, 2 s and 2.0 eV steps were used, and from 20150 to 21200 eV, 4 s and 4.0 eV were used. For the 5MoC/ NaHY-9 sample, 12 spectra were recorded to improve the signal-to-noise ratio. The EXAFS data were treated by standard procedures, by using the IFEFFIT software to extract and simulate the EXAFS spectra. Structural parameters were obtained from the best fit in R space (Fourier transformed), making use of phase functions and amplitudes calculated by the FEFF 8.20 program.[15] The resulting parameters were named in the same way as in the FEFFIT code,[16] namely, CN = coordination number, R = interatomic distance, σ^2 = Debye−Waller factor, S_0^2 = multielectronic factor, and R_{factor}, which is related to the quality of the fit, i.e., the agreement of simulated and experimental curves. The R_{factor} is expressed as

$$R_{\text{factor}}\,(\%) = \frac{\sum(k^3\chi(\mathbf{k})_{\text{exptl}} - k^3\chi(\mathbf{k})_{\text{sim}})^2}{\sum(k^3\chi(\mathbf{k})_{\text{exptl}})^2} \times 100$$

where $\chi(\mathbf{k})$ describes the EXAFS oscillation as a function of the wave vector $\mathbf{k}$.

X-ray absorption spectra at the molybdenum L_{II} and L_{III} edges (ca. 2520 eV) were also obtained at the LNLS using a soft X-ray line. The measurements were performed in an ultra-high-vacuum chamber in total electron yield (TEY) mode, using a Si (111) monochromator and ca. 1.8 eV resolution. The samples in powder form were mounted on double-faced conducting carbon adhesive tape. The carburized samples were always manipulated under an argon atmosphere and, after being mounted on the adhesive tape, were covered with isooctane to minimize exposure to air. The isooctane was removed by evaporation in the vacuum chamber of the soft X-ray line. The spectra were taken in the 2500−2690 eV range. In the regions where X-ray absorption occurs (2515−2534.8 and 2615−2639.8 eV), 1 s, 0.2 eV steps were used, and 1 s, 1 eV steps were used elsewhere.

Molybdenum hexacarbonyl, molybdenum(VI) oxide, passivated β-molybdenum carbide, and sodium molybdate were used as standards in both EXAFS and XANES measurements.

TABLE 1: Characteristics of the Catalysts

catalyst	S_{BET}[a]/ $m^2\ g^{-1}$	$Q_a(CO)$[b]/ $\mu mol\ g^{-1}$	CO/Mo[c]	Mo/C[d]
5MoCI/NaHY-9	486	25.1	0.048	3.8
5MoC/NaHY-9	546	81.1	0.16	3.4
10MoC/NaHY-9	485	107.4	0.10	2.3

[a] Surface area measured by the BET method. [b] Irreversibly chemisorbed CO at 308 K. [c] Ratio of chemisorbed CO to molybdenum atoms. [d] Molybdenum/carbon ratio measured by the reoxidation procedure.

2.4. Theoretical Calculations. DFT was used to perform quantum mechanical calculations, within the B3LYP exchange-correlation functional. The basis set used was 6-31G** for all but molybdenum atoms. For molybdenum the SBKJC effective core potential was used to treat inner-shell electrons. The zeolite was treated as a t4 cluster model with one aluminum atom and one sodium as the charge-compensating cation. Geometry optimization was done by allowing all degrees of freedom to relax, which means that none of the bond lengths and angles were constrained to keep a fixed value. All the calculations were done with the GAMESS package.[17]

3. Results and Discussion

The results for surface area, chemisorption of carbon monoxide, and carbon content for carburized samples are shown in Table 1. Some decrease is observed in the surface area of the catalysts when compared to that of the original zeolite, especially if the area per unit mass of the support is considered. This decrease is small enough for one to conclude that the structure of the support was largely preserved during the metal incorporation and carburization.

All three catalysts adsorb carbon monoxide irreversibly at 308 K. This chemisorption is related to the presence of the carburized molybdenum, since it does not occur on the pure zeolite. In what concerns the ratio of chemisorbed carbon monoxide to molybdenum atoms, there is a remarkable difference among the materials, that is, 5MoC/NaHY-9 > 10MoC/NaHY-9 > 5MoCI/NaHY-9. The catalyst obtained by impregnation chemisorbs only 1/3 of the amount observed with the one produced by adsorption of hexacarbonyl having the same content of molybdenum. All catalysts contain a significant amount of carbon, with 10MoC/NaHY-9 having a Mo/C ratio close to that of the bulk carbide, i.e., 2/1.

The catalysts were tested in benzene hydrogenation at 363 K, and the results of conversion as a function of time are shown in Figure 1. The catalyst 10MoC/NaHY-9 presents the highest initial activity, although it suffers rapid deactivation, and after 2 h of reaction, the conversion was nearly zero. The 5MoCI/NaHY-9 catalyst has the next highest initial activity, but it also undergoes pronounced deactivation and, after 2.5 h, converts only about 8% of the benzene to cyclohexane. In contrast, the 5MoC/NaHY-9 catalyst, despite having the lowest initial activity, after 2.5 h of reaction achieves a nearly stable activity with a conversion of about 16%. The different deactivation patterns of 5MoC/NaHY-9, 5MoCI/NaHY-9, and 10MoC/NaHY-9 suggest that the active phases in each of them are different.

The ^{27}Al NMR spectrum of the pure zeolite indicated the presence of EFAL, associated with a peak with a shift around 0 ppm, which is typical of aluminum in octahedral coordination, as shown in Figure 2a. Figure 2b shows the spectrum of the precursor of 5MoCI/NaHY-9. This precursor was obtained by calcination after impregnation with AHM and is named MoO_3/NaHY-9.

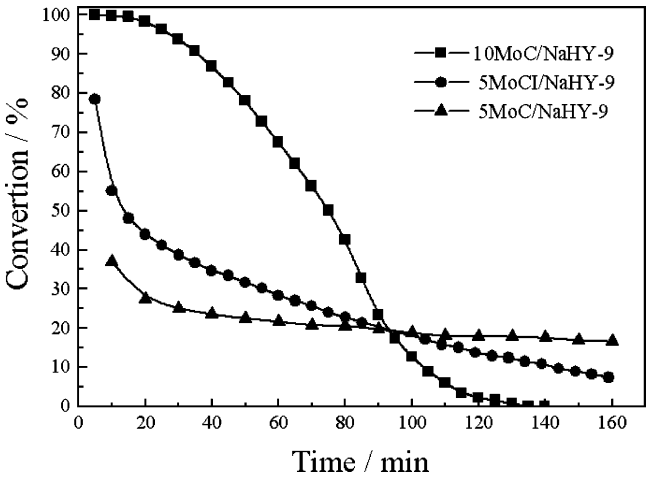

Figure 1. Benzene hydrogenation activity at 363 K and atmospheric pressure for catalysts 5MoC/NaHY-9, 10MoC/NaHY-9, and 5MoCI/NaHY-9.

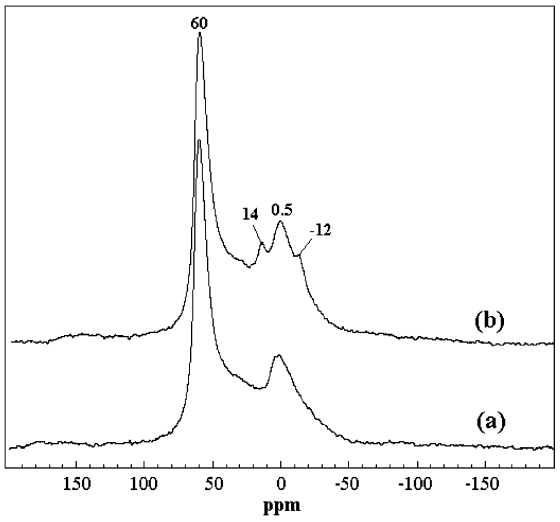

Figure 2. ^{27}Al NMR spectrum of the precursor prepared by impregnation with AHM solution followed by calcination (b) as compared to that of the parent zeolite (a).

In the spectrum of the precursor, two peaks not originally present in the zeolite support could be detected around 14 and −12 ppm, which are typical of aluminum in octahedral sites and which have been attributed to an Anderson heteropolymolybdate, $[Al(OH)_6Mo_6O_{18}]^{-3}$, and to aluminum molybdate, $Al_2(MoO_4)_3$, respectively.[18−20] The formation of such species indicates that, after impregnation and calcination, the EFAL of the zeolite support interacts with molybdenum, forming mixed molybdenum−aluminum species.

The NMR spectra of the carburized catalysts are shown in Figure 3a. For all samples, a strong decrease in the intensity of the peak at 0 ppm has occurred, as compared to that of the pure zeolite. This behavior may not be attributed to the disappearance of EFAL nor to realumination of the zeolite framework, but to the formation of disordered aluminum species not detectable by NMR, the so-called "invisible aluminum".[21] The loss of coordination symmetry around the aluminum atoms due to structural disorder causes a large increase in the aluminum nuclear quadrupolar coupling constant, and consequently, the peaks become too broad for observation.[21]

To corroborate the presence of invisible aluminum species in the carburized catalysts, impregnation of 5MoC/NaHY-9 and 10MoC/NaHY-9 with a 38% solution of acetylacetone (ACAC)

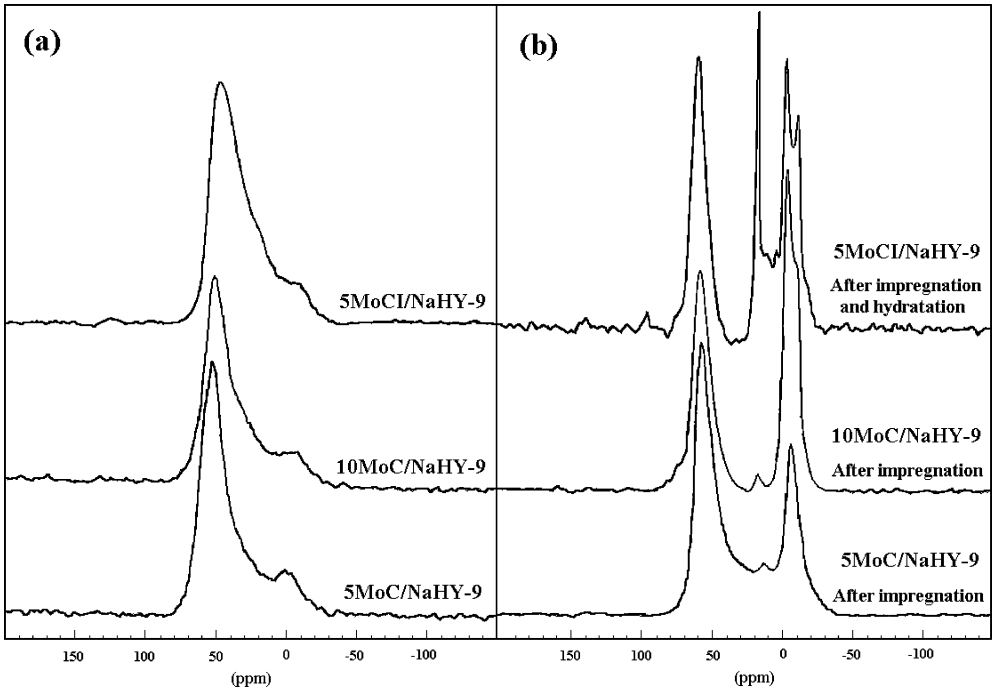

Figure 3. ^{27}Al NMR spectra of the carburized catalysts (a) and the same samples after hydration and/or complexation with acetylacetone (b).

in ethanol was carried out for 3 h, followed by drying and new acquisition of the ^{27}Al spectrum. The 5MoC/NaHY-9 sample was additionally rehydrated by addition of two drops of water, after the impregnation with ACAC. The results are shown in Figure 3b.

When the carbided catalysts are contacted with acetylacetone, there is a large increase in the ^{27}Al NMR peak at 0 ppm generally attributed to EFAL. This is caused by restoration of octahedral symmetry around the aluminum atoms due to complexation by ACAC.[22]

For 5MoC/NaHY-9, as a consequence of the impregnation procedure with ACAC, one can observe the presence of a small peak at 15 ppm, typical of Anderson's anion, and another broad and intense peak at −4 ppm. In the 10MoC/NaHY-9 sample, in addition to these two, an intense but not completely resolved peak appeared around −12 ppm. Finally, in the 5MoCI/NaHY-9 sample these three peaks are very sharp and well resolved.

We have not found in the literature references about the formation of complexes involving EFAL and ACAC with so distinct chemical shifts in ^{27}Al NMR, such as to justify the formation of two well-resolved peaks at −4 and −12 ppm. One plausible explanation is that the peak at −4 ppm is associated with boehmite-type aluminum complexed to ACAC and the one at −12 ppm to aluminum species in an environment similar to that of aluminum molybdate. It is interesting that reaction with ACAC leads to production of a compound that does not require an ACAC ligand to be formed. We believe this is caused by oxidation of reduced molybdenum in a mixed Mo−Al species by the acidic protons in ACAC, which may be formally represented by reaction 1. This reaction is more efficient than oxidation with water, since ACAC is a stronger acid than water.

$$(6-x)CH_2(CH_3CO)_2 + Mo^{x+} \rightleftarrows Mo^{6+} + (6-x)[CH(CH_3CO)_2]^- + H_2 \quad (1)$$

Therefore, in 5MoC/NaHY-9, practically all aluminum in octahedral sites is present as EFAL, in a boehmite-like structure, with only a small portion of the species in interaction with molybdenum. On the other hand, in 5MoCI/NaHY-9, an appreciable amount of EFAL is interacting with molybdenum. An intermediate situation is found with 10MoC/NaHY-9.

The interaction between molybdenum and aluminum in the 5MoCI/NaHY-9 catalyst is not surprising, considering that Mo−Al interaction was already present in the MoO_3/NaHY-9 calcined precursor before carburization, as shown in Figure 3b. Zeolites are cation exchangers, and molybdenum cannot exchange with the charge compensation cations in anionic form, such as in molybdates and polymolybdates, when its incorporation is done by the impregnation method. It may however deposit at the zeolite mesopores during drying and interact with EFAL during the subsequent calcination. Some of the molybdenum may even diffuse to the interior of the zeolite cages during high-temperature treatment due to the volatility of molybdenum(VI) oxide.[23]

Figure 4 shows the XANES spectra of the catalysts and standards near the molybdenum L_{III} absorption edge in the region of 2515−2535 eV. Prominent in these spectra is the "white line" that corresponds to transition of a molybdenum $2p_{3/2}$ electron to empty 4d levels. Transition of a $2p_{1/2}$ electron to 4d levels gives rise to the white line in the L_{II} absorption edge in the 2620−2640 eV range. The line shapes for both edges are very similar to each other and provide the same electronic and structural information. Therefore, in this work only the results corresponding to the L_{III} edge are presented and discussed.

It is well-known that the absorption edge shifts to higher energy as the oxidation state of the absorbing atom increases. This is clearly apparent from Figure 4, as we compare the spectra corresponding to molybdenum metal and molybdenum carbide on one hand (zero formal oxidation state) and molybdenum oxide and sodium molybdate on the other (+6 formal oxidation state). Furthermore, the white line for Mo^{6+} is seen to consist of a doublet. When the molybdenum is octahedrally coordinated to oxygen, the proportion of the low-energy component to the high-energy component is ca. 3/2 and the separation between them is 3.1−4.5 eV,[24,25] close to the 3.2 eV obtained from our

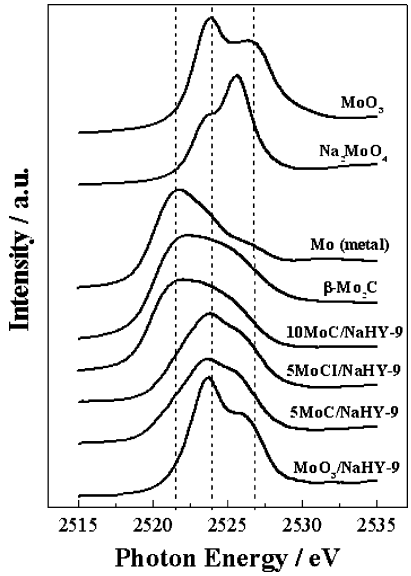

Figure 4. XANES spectra of standards and carburized catalysts near the molybdenum L_{III} absorption edge.

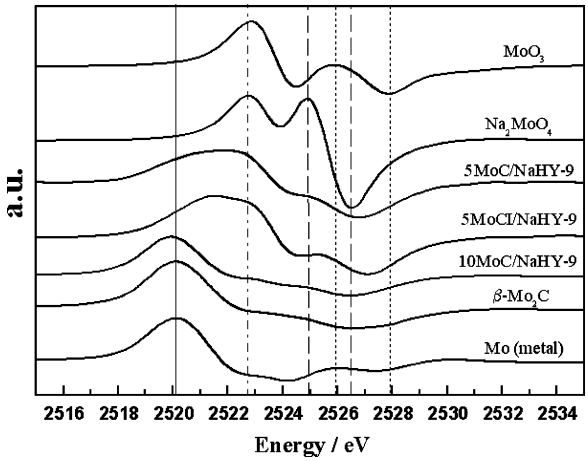

Figure 5. First-derivative XANES spectra of standards and carburized catalysts near the molybdenum L_{III} absorption edge.

data. These features correspond respectively to the degeneracy and energy split of t_{2g} and e_g 4d orbitals in an octahedral ligand field. Similarly, the ca. 2/3 ratio and 2.3 eV energy separation observed with sodium molybdate correspond respectively to the degeneracy and energy split of e and t_2 4d orbitals in a tetrahedral ligand field, reported as 1.8−2.6 eV.[24,25]

With the exception of 10MoC/NaHY-9, the spectra of all carburized catalysts have a maximum at nearly the same position as the first maximum in the MoO_3 and sodium molybdate doublets, but the separation between the two components is not as clear as in the standard compounds, and their absorption threshold occurs at lower energy. This suggests that, in 5MoC/NaHY-9 and 5MoCI/NaH-9, the molybdenum species are predominantly in an oxidation state higher than that of molybdenum carbide, but lower than that of MoO_3 and Na_2MoO_4. This is more clearly apparent in the first-derivative spectra shown in Figure 5.

The first maximum in each derivative spectrum corresponds to the L_{III} absorption edge. With the Mo^{6+} compounds, a second maximum is observed that corresponds to the absorption edge of the high-energy component of the doublet. On the other hand, the spectrum of the catalyst containing 10% molybdenum, 10MoC/NaHY-9, is nearly identical to that of β-Mo_2C, with a

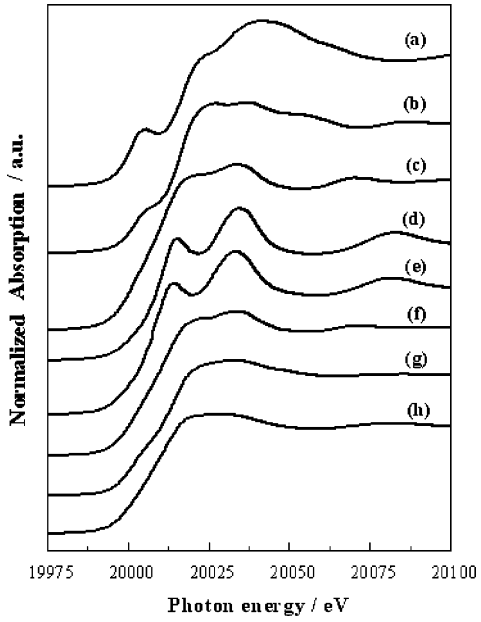

Figure 6. XANES spectra of standards and carburized catalysts near the molybdenum K absorption edge: Na_2MoO_4 (a), MoO_3 (b), β-Mo_2C (c), $Mo(CO)_6$ (d), $5Mo(CO)_6$/NaHY-9 (e), 10MoC/NaHY-9 (f), 5MoC/NaHY-9 (g), 5MoCI/NaHY-9 (h).

first maximum at the same energy (the spectra were vertically scaled to facilitate visualization). The derivative spectra of catalysts 5MoC/NaHY-9 and 5MoCI/NaHY-9 present a first maximum at an energy greater than that of the carbide but lower than that of the oxide and a second maximum at an energy similar to that of the oxide species.

Figure 6 shows the XANES spectra of the catalysts and standards at the molybdenum K edge. Comparison with the spectrum of molybdenum hexacarbonyl shows that the complex is decomposed due to carburization of the precursors during the preparation of 5MoC/NaHY-9 and 10MoC/NaHY-9 catalysts. As in the case of the L edge spectra, the 10MoC/NaHY-9 spectrum is virtually identical to that of β-Mo_2C. The spectra of 5MoC/NaHY-9 and 5MoCI/NaHY-9 catalysts have small differences between them and do not present resemblance either to the bulk carbide or to the oxides, which indicates that, for these samples, molybdenum is in a distinct chemical state. The absence of any preedge peak or shoulder renders these spectra closer to those of compounds where molybdenum is in a low state of oxidation than to those of the Mo^{6+} compounds. The spectrum of the precursor of 5MoC/NaHY-9 catalyst, named $5Mo(CO)_6$/NaHY-9, is also shown, and it is very similar to the spectrum of the pure molybdenum hexacarbonyl, which indicates that the complex is adsorbed without decomposition within the zeolite cavities.

To carry out a more detailed analysis, EXAFS spectra were recorded. The standards used were passivated β-Mo_2C ($P6_3/mmc$), Na_2MoO_4 ($Fd3m$), and the precursor of 5MoC/NaHY-9 catalyst. The latter was used as a standard in place of the hexacarbonyl itself, since it was verified, from the K edge XANES spectra, that molybdenum hexacarbonyl keeps its structure after adsorption on the zeolite, in agreement with the literature.[26]

Figure 7 shows the EXAFS oscillations and Fourier-transformed spectra at the molybdenum K edge between 0 and 6 Å for the standards and the $5Mo(CO)_6$/NaHY-9 precursor. The β-molybdenum carbide presents a small peak around 2 Å characteristic of carbon as a first nearest neighbor, a large second peak related to Mo around 3 Å as a second nearest neighbor,

TABLE 2: Results for EXAFS Simulation of the Standards Using $S_0^2 = 0.92$

sample	path[a]	CN[b]	r/Å	σ^2/Å^2	R_{factor}/ %	E_0/eV
β-Mo_2C	Mo−C	3	2.090 ± 0.004	0.004 ± 0.002	2.7	4.5 ± 1.4
	Mo−Mo	12	2.966 ± 0.030	0.009 ± 0.0003		
Na_2MoO_4	Mo−O	4	1.773 ± 0.007	0.002 ± 0.0008	2.8	2.6 ± 1.9
5Mo(CO)$_6$/NaHY-9	Mo−C	6	2.064 ± 0.010	0.004 ± 0.0009	3.0	−3.3 ± 1.5
	Mo−O	6	3.249 ± 0.023	0.0001 ± 0.0001		

[a] Scattering path. [b] Fixed coordination number.

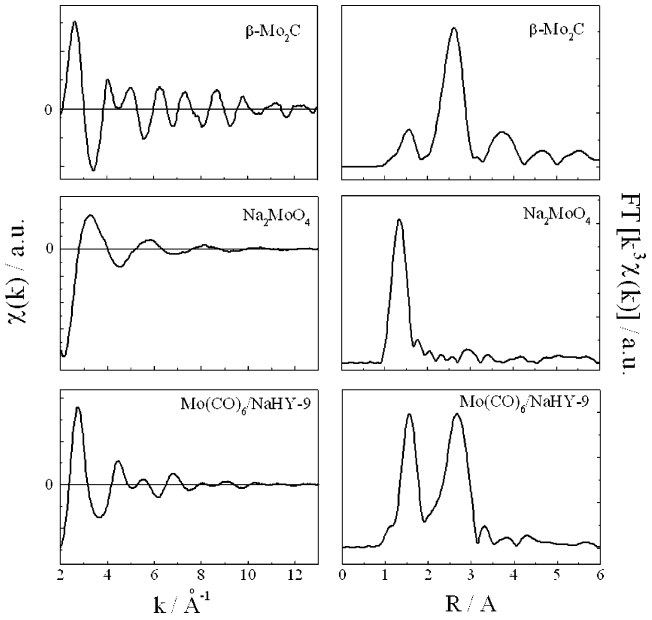

Figure 7. Experimental EXAFS oscillations (left) and k^3-weighted Fourier-transformed spectra (right) for the standards.

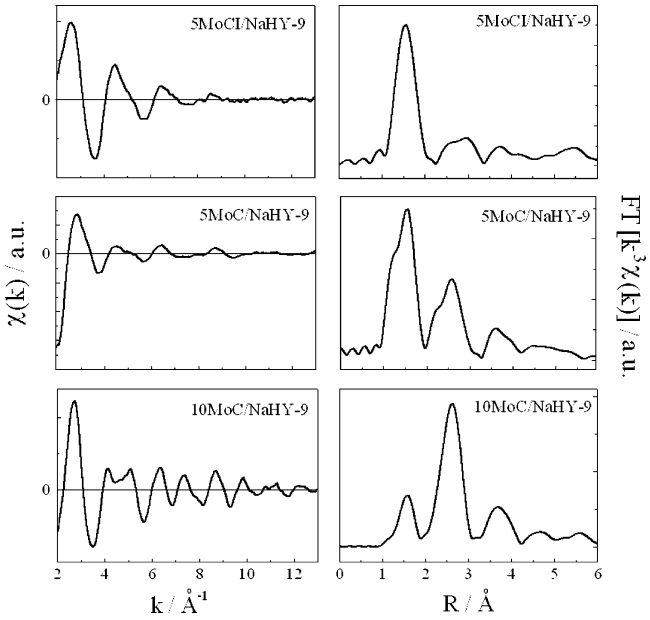

Figure 8. Experimental EXAFS oscillations (left) and k^3-weighted Fourier-transformed spectra (right) for the carburized catalysts.

and other smaller peaks characteristic of Mo as more distant neighbors. Sodium molybdate presents a simple spectrum formed by one sphere of coordination at a distance smaller than 2 Å, characteristic of oxygen atoms. Finally, the spectrum of adsorbed molybdenum hexacarbonyl presents two peaks around 2 and 3 Å, attributed to carbon and oxygen atoms as first and second nearest neighbors, respectively.

For the simulation of the EXAFS spectra of the standards, a value of 0.92 was used for the S_0^2 parameter, obtained from the simulation of the spectrum of sodium molybdate, where this parameter was free to float. This value is very close to the one calculated theoretically by the FEFF program (0.936). Thus, by using this value and keeping the coordination number of molybdenum constant in each case, the simulation of EXAFS data for the standards was performed, considering only single scattering paths. The numerical simulation results obtained are presented in Table 2. The simulation may be considered very satisfactory, since the parameters indicative of the quality of the fits, namely, R_{factor}, E_0, and σ^2, are in the range accepted.[15,16]

The EXAFS oscillations and Fourier-transformed spectra for the carburized catalysts are shown in Figure 8. It is clear that the molybdenum environment is distinct in each case. With 5MoCI/NaHY-9, a single peak around 1.7 Å dominates the radial distribution function and its magnitude is rather small. With 5MoC/NaHY-9, a peak corresponding to a second coordination sphere is clearly observed at ca. 2.5 Å. A peak at approximately the same distance is larger than the one corresponding to the first coordination sphere in the spectrum of 10MoC/NaHY-9.

Although EXAFS is a powerful technique, other information about the studied systems is necessary. In the present case, it was already known that all catalysts have a certain amount of carbon, which opens the possibility of Mo−C scattering paths. From the XANES results for 10MoC/NaHY-9, the presence of molybdenum carbide in this catalyst was confirmed. From ^{27}Al NMR for 5MoCI/NaHY-9, we could infer the existence of molybdenum atoms in the vicinity of aluminum. Thus, EXAFS analysis at the molybdenum edge for this sample had to include Mo−Al scattering paths.

Keeping these points in mind, the FEFF simulations for the EXAFS spectra of the three catalysts were performed. The results are shown in Figure 9 and the corresponding parameters in Table 3. It is clear from Figure 9 that, with 10MoC/NaHY-9, the Mo−C distances and coordination numbers for the first coordination sphere are consistent with the predominance of molybdenum carbide in this catalyst. However, the coordination number for the second coordination sphere (Mo−Mo distances) is smaller than the one expected for bulk molybdenum carbide, which should be 12 rather than 9. This is probably due to the fact that the molybdenum carbide particles are so small that a large fraction of them are at the surface and are therefore coordinatively unsaturated. A simplified model was constructed to estimate the size of the particles, based on the hexagonal close-packed structure of the molybdenum atoms in β-molybdenum carbide. The molybdenum atoms are assumed to be located at the corners of trigonal prisms with an extra molybdenum atom at the center. Three of these prisms share a common edge to form a hexagonal prism, which is assumed to be the elementary particle. As shown in Figure 10, the elementary particles H1 are assumed to grow keeping the hexagonal prism shape, resulting in particles H2 and H3 successively. From this model, an average number of 9 molybdenum atoms in the

TABLE 3: EXAFS Simulation Parameters for Carburized Catalysts

sample	path[a]	CN	r/Å	σ^2/Å^2	R_{factor}/ %	E_0/eV
5MoCI/NaHY-9	Mo−O	1.5 ± 0.3	2.053 ± 0.024	0.002	2.8	1.3 ± 2.4
	Mo−C	1.0 ± 0.5	2.251 ± 0.085	0.004		
	Mo−Al	1.6 ± 1.5	3.426 ± 0.035	0.008		
5MoC/NaHY-9	Mo−C	1.0 ± 0.4	1.758 ± 0.009	0.001	4.3	−1.4 ± 3.4
	Mo−O	1.9 ± 0.7	2.025 ± 0.023	0.012		
	Mo−Mo	1.0 ± 0.6	2.921 ± 0.019	0.008		
10MoC/NaHY-9	Mo−C	2.8 ± 0.6	2.095 ± 0.016	0.004	3.4	−2.5 ± 1.6
	Mo−Mo	8.8 ± 0.6	2.967 ± 0.008	0.009		

[a] Scattering path.

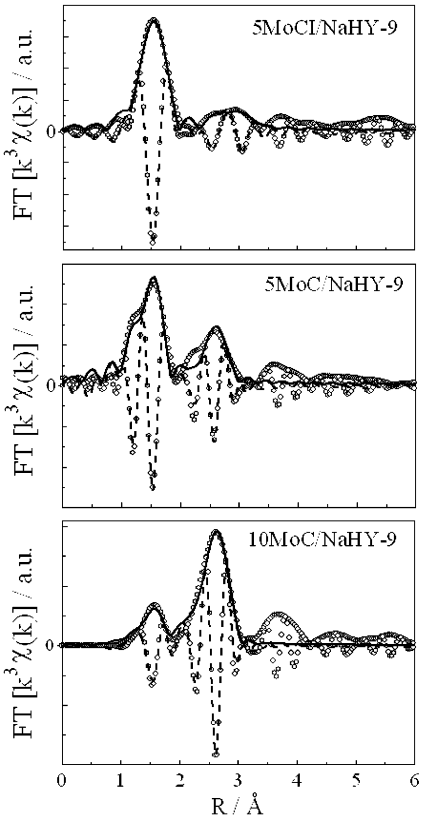

Figure 9. Magnitude (solid line) and imaginary (dashed line) parts of the Fourier-transformed spectra for the carburized catalysts: open circles, experimental; line, simulated.

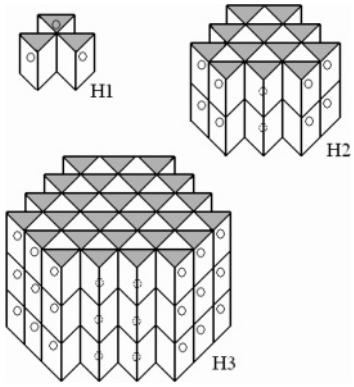

Figure 10. Hexagonal-prism model to estimate the size of the molybdenum carbide particles (see the text).

second coordination sphere is consistent with a particle having 229 molybdenum atoms and ca. 1.8 nm diameter, H3 in the figure.

To simulate the spectrum of the 5MoCI/NaHY-9 sample, it was necessary to include a Mo−Al scattering path in the FEFF simulations, using the Mo−Al bond distance in β-aluminum molybdate, which has an orthorhombic structure and belongs to space group *Pbcn* (No. 60), $a = 12.5547$ Å, $b = 9.0214$ Å, and $c = 9.1035$ Å. From the R_{factor} obtained and the curve shown in Figure 9, the results obtained are of good quality. Apparently the molybdenum atoms are essentially isolated from each other and belong to a mixed aluminum−molybdenum oxycarbide, probably produced by interaction with the EFAL. From the available results, the detailed structure of this phase is uncertain, but it must be highly disordered, since it is not detectable by ^{27}Al NMR. It should be stressed that omission of the Mo−Al path or its replacement by a Mo−Mo path strongly impaired the quality of the fit.

At this point, the structure of the molybdenum species in 5MoC/NaHY-9 was not completely clarified. The EXAFS simulation, however, furnishes average distances and coordination numbers for Mo−C, Mo−O, and Mo−Mo bonds (see Table 3). It is worth emphasizing that these are average distances, since only two bond distances were allowed for the first molybdenum coordination sphere.

The parameters obtained from the FEFF simulations for catalyst 5MoC/NaHY-9 are close to the ones reported by Iwasawa's group[26−28] for the molybdenum species obtained by vacuum decomposition of molybdenum hexacarbonyl adsorbed on a NaY zeolite. They proposed that this species consists of a Mo_2C unit bound to the oxygen atoms of the zeolite framework. To verify whether this dimer species could be present in catalyst 5MoC/NaHY-9, we performed theoretical calculations at the DFT/B3LYP level. After several trial structures, we found one which has geometric parameters quite compatible with those obtained from the EXAFS simulation. This structure is displayed in Figure 11a, and Table 4 shows the main bond distances. It consists of Mo_2CO_4 units bound to two oxygen atoms of the zeolite framework. Its structure resembles that of β-Mo_2C, as can be seen from Figure 11b. The difference is that some carbon positions are exchanged with oxygen while others are missing. The average coordination numbers of molybdenum, both to carbon and to oxygen, are consistent with the ones obtained from the FEFF simulations, bearing in mind the uncertainty in the simulation parameters.

The dimer structure presented in Figure 11a has a triplet ground state. The corresponding singlet state is about 15 kcal/mol above. The presence of paramagnetic species in the catalysts was pointed out in a previous work.[13] Also in this dimer, the average oxidation state of molybdenum is higher than in molybdenum carbide, which is consistent with the XANES spectra at the molybdenum L edge. Therefore, the proposed species, besides representing an energy minimum, seems to accommodate the known experimental facts. It is worth noting

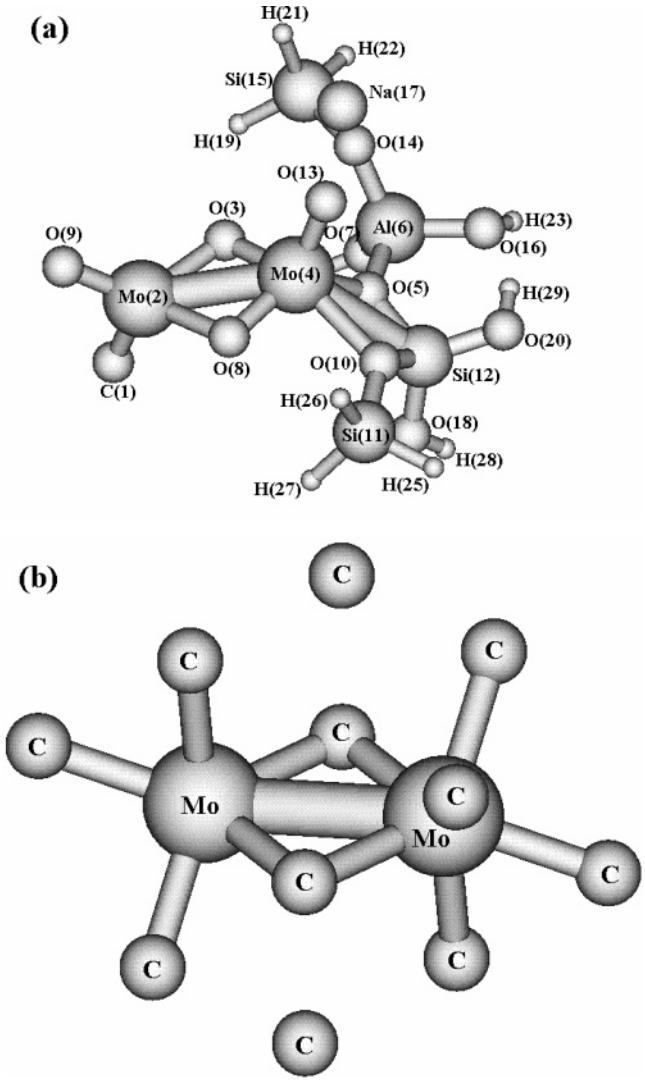

Figure 11. Carbide and oxycarbide structures: (a) structure of calculated dimer species; (b) idealized local structure of β-molybdenum carbide. In the real structure half of the carbon atoms are missing.

TABLE 4: Interatomic Distances Calculated by DFT for the Dimer Species[a]

path	R_{calcd}/ Å	path	R_{calcd}/ Å
Mo(2)−C(1)	1.79	Mo(4)−O(3)	1.89
Mo(2)−O(3)	2.07	Mo(4)−O(5)	2.13
Mo(2)−O(8)	2.09	Mo(4)−O(8)	1.86
Mo(2)−O(9)	1.73	Mo(4)−O(10)	2.33
Mo(2)−Mo(4)	2.97	Mo(4)−O(13)	1.75
Mo(4)−Mo(2)	2.97		

[a] The numbers in parentheses refer to those in Figure 11.

that changing the position of the carbon atom in the dimer causes little variation in energy, so it is possible that a distribution of isomeric species with the same basic structure actually exists in the catalyst.

It should also be pointed out that, if a species similar to the one proposed by Iwasawa's group[26−28] is considered, where all of the oxygen atoms belong to the zeolite framework, an energy minimum is not obtained, and removal of the bridging oxygen atoms between the molybdenum atoms brings about a large decrease in the Mo−Mo distance, leading to values that are not compatible with the EXAFS results.

It is interesting that using the same preparation method and the same zeolite as the support, only doubling the molybdenum loading, as in catalysts 5MoC/NaHY-9 and 10MoC/NaHY-9, completely changes the character of the predominant supported molybdenum species. This could be due to a nucleation and growth type of phenomenon. As molybdenum carbide is a highly refractory material, it should have a large excess surface energy. It is possible that small molybdenum carbide clusters are not stable and decompose to form the dimer species. Above a certain critical size, carbide particles may become stable, and apparently the critical concentration for that to occur should be between 5 and 10 wt % molybdenum.

From the characterization results, it is not surprising that the three catalysts have such different catalytic behaviors in benzene hydrogenation, with respect to both activity and stability, since the predominant molybdenum species is very distinct in each one of them.

4. Conclusions

Changing the molybdenum incorporation method (adsorption of molybdenum hexacarbonyl or impregnation with ammonium heptamolybdate solution) and the molybdenum loading (5 or 10 wt % Mo) of carburized Y zeolite-supported catalysts caused pronounced differences in catalytic activity and stability in benzene hydrogenation at atmospheric pressure and 363 K. The initially most active catalyst was the one containing 10 wt % molybdenum and prepared by hexacarbonyl adsorption, followed by the one prepared by impregnation and finally by the one containing 5 wt % molybdenum and prepared by hexacarbonyl adsorption. The catalytic stability followed the reverse order, so after a few hours on stream the activity order was also reversed.

Characterization results by ^{27}Al solid-state NMR and X-ray absorption techniques showed that these differences in catalytic behavior may be explained by pronounced differences in the nature of the predominant supported molybdenum species. With catalyst 10MoC/NaHY-9, the predominant species is β-molybdenum carbide nanocrystals. With 5MoCI/NaHY-9, the predominant species seems to be a mixed aluminum−molybdenum oxycarbide. In 5MoC/ NaHY-9 a dimeric molybdenum oxycarbide with composition Mo_2CO_4 and bound to oxygen atoms of the zeolite framework is proposed to be the main supported species on the basis of both EXAFS characterization and theoretical calculations using density functional theory.

Acknowledgment. We acknowledge financial support by FINEP and PETROBRAS through the CTPETRO fund. A.S.R. thanks the Agência Nacional do Petróleo, ANP, for a doctorate scholarship. We also thank the Conselho Nacional de Desenvolvimento Científico e Tecnológico of Brasil (CNPq) and the LNLS for XAS measurements.

References and Notes

(1) Levy, R. B.; Boudart, M. *Science* **1973**, *181*, 547.
(2) Oyama, S. T. *Catal. Today* **1992**, *15*, 179.
(3) Neylon, M. K.; Choi, S.; Kwon, H.; Curry, K. E. *Appl. Catal., A* **1999**, *183*, 253.
(4) St. Clair, T. P.; Dhandapani, B.; Oyama, S. T. *Catal. Lett.* **1999**, *58*, 169.
(5) Solymosi, F.; Cserényi, J.; Szöke, A.; Bánsági, T.; Oszkó, A. *J. Catal.* **1997**, *165*, 150.
(6) Wang, D.; Lunsford, J. H.; Ronynek, M. P. *J. Catal.* **1997**, *169*, 347.
(7) Liu, S.; Wang, L.; Ohnishi, R.; Ichikawa, M. *J. Catal.* **1999**, *181*, 175.
(8) Ding, W.; Li, S.; Meitzner, G. D.; Iglesia, E. *J. Phys. Chem. B* **2001**, *105*, 506.
(9) Yuan, S.; Hamid, S. B. D.-A.; Li, Y.; Ying, P.; Xin, Q.; Derouane, E. G.; Li, C. *J. Mol. Catal. A* **2002**, *184*, 257.

(10) Barbier, J.; Lamy-Pitara, E.; Marecot, P.; Boitiaux, J. P.; Cosyns, J.; Verna, F. *Adv. Catal.* **1990**, *37*, 279.
(11) Yasuda, H.; Yoshimura, Y. *Catal. Lett.* **1997**, *46*, 43.
(12) Yasuda, H.; Sato, T.; Yoshimura, Y. *Catal. Today* **1999**, *50*, 71.
(13) Rocha, A. S.; da Silva, V. L. T.; Leitão, A. A.; Herbst, M. H.; Faro, A. C., Jr. *Catal. Today* **2004**, *98*, 281.
(14) Zotin, J. L. Thèse de Doctorat, Université Claude Bernard—Lyon I, France, 1993.
(15) Ankudinov, A. L.; Ravel, B.; Rehr, J.J.; Conradson, S. D. *Phys. Rev. B* **1998**, *58*, 7565.
(16) Newville, M.; Ravel, B.; Haskel, D.; Rehr, J. J.; Stern, E. A.; Yacoby, Y. *Physica* **1995**, *B208* and *B209*, 154.
(17) Schmidt, M. W.; Baldridge, K. K.; Boatz, J. A.; Elbert, S. T.; Gordon, M. S.; Jensen, J. H.; Koseki, S.; Matsunaga, N.; Nguyen, K. A.; Su, S. J.; Windus, T. L.; Dupuis, M.; Montgomery, J. A. *J. Comput. Chem.* **1993**, *14*, 1347.
(18) Plazenet, G.; Payen, E.; Lynch, J.; Rebours, B. *J. Phys. Chem. B* **2002**, *106*, 7013.
(19) Klimova, T.; Calderón, M.; Ramírez, J. *Appl. Catal., A* **2003**, *240*, 29.
(20) Klimova, T. *Appl. Catal., A* **2003**, *253*, 321.
(21) Freude, D.; Fröhlich, T.; Pfeifer, H.; Scheler, G. *Zeolites* **1983**, *3*, 171.
(22) Bosacek, V.; Freude, D.; Fröhlich, T.; Pfeifer, H.; Schmiedel, H. *J. Colloid Interface Sci.* **1982**, *85*, 502.
(23) Leyrer, J.; Zaki, M. I.; Knözinger, H. *J. Phys. Chem.* **1986**, *90*, 4475.
(24) Bare, S. R.; Mitchell, G. E.; Maj, J. J.; Vrieland, G. E.; Gland, J. L. *J. Phys. Chem.* **1993**, *97*, 6048−128.
(25) Lede, E. J.; Requejo, F. G.; Pawelec, B.; Fierro, J. L. G. *J. Phys. Chem. B* **2002**, *106*, 7824.
(26) Asakura, K.; Noguchi, Y.; Iwasawa, Y *J. Phys. Chem. B* **1999**, *103*, 1051.
(27) Shido, T.; Asakura, K.; Noguchi, Y.; Iwasawa, Y *Appl. Catal., A* **2000**, *194*−*195*, 365.
(28) Yamaguchi, A.; Suzuki, A.; Shido, T.; Inada, Y.; Asakura, K.; Nomura, M.; Iwasawa, Y *J. Phys. Chem. B* **2002**, *106*, 2415.